Geophysical Journal International

Geophys. J. Int. (2015) **203,** 2049–2054 doi: 10.1093/gji/ggv421
GJI Seismology

Stochastic characterization of mesoscale seismic velocity heterogeneity in Long Beach, California

Nori Nakata and Gregory C. Beroza
Stanford University, Stanford, CA, USA. E-mail: nnakata@stanford.edu

Accepted 2015 September 28. Received 2015 September 23; in original form 2015 July 23

SUMMARY

Earth's seismic velocity structure is heterogeneous at all scales, and mapping that heterogeneity provides insight into the processes that create it. At large scale lengths, seismic tomography is used to map Earth structure deterministically. At small scale lengths, structure can be imaged deterministically, but because it is impractical to image short-wavelength heterogeneity everywhere, we often resort to statistical methods to depict its variability. In this study, we develop random-field model representations of a 3-D *P*-wave velocity model at Long Beach, California, estimated from dense-array recordings of the ambient seismic wavefield. We focus on heterogeneity at the mesoscale, which is smaller than 10+ km scale of regional tomography but larger than the *micro* scale of borehole measurements. We explore four ellipsoidally anisotropic heterogeneity models, including von Kármán, Gaussian, self-affine and Kummer models, based on their autocorrelation functions. We find that the von Kármán model fits the imaged velocity model best among these options with a correlation length in the horizontal direction about five times greater than in the vertical direction, and with strong small-scale length variations. We validate our results by showing that our model accurately predicts the observed decay of scattered waves in the coda of a nearby earthquake, suggesting that quantitative measures of velocity variability will be useful for predicting high-frequency ground motion in earthquakes.

Key words: Spatial Analysis; Fractals and multifractals; Probability distributions; Earthquake ground motions; Coda waves; Statistical seismology.

INTRODUCTION

The Earth's interior contains heterogeneity at various scales. Seismic tomography is the primary technique to estimate velocity heterogeneity (Aki *et al.* 1976); however, it can also be measured more directly in the near surface using logging techniques (Holliger 1996; Shiomi *et al.* 1997). For small-scale heterogeneities, stochastic representations are a powerful method to extend interpretation to volumes that are impractical to model deterministically. Moreover, stochastic representations can yield additional insights. For example, Holliger & Levander (1992) found that the small-scale geologic features correlate with regional tectonics. Levander & Holliger (1992) and Holliger & Levander (1994) estimated the randomness of a medium from waves reflected in the lower crust to understand how laminated structures, including the Moho, are formed. Statistical properties of the seafloor morphology are related to processes of seafloor formation at the ridge crest, tectonics, and post-depositional transport (Goff & Jordan 1988). Shiomi *et al.* (1997) speculated that the difference in power-law behaviour of different regions is related to tectonics. Gudmundsson *et al.* (1990) found that global traveltime residuals contain heterogeneities and random errors, and that large heterogeneities tend to concentrate at upper-mantle zones. Puster & Jordan (1997) developed a relationship between tomographic velocity models and mantle dynamics, such as the degree of stratification in mantle flow, using the correlation length of heterogeneity. Becker *et al.* (2007) used stochastic modelling of shear-wave splitting to characterize continental lithosphere and upper mantle, and found that the correlation length of the heterogeneity of the splitting relates to geological features.

Such small-scale heterogeneities are also important to explain seismic coda waves and wave propagation (Aki 1969; Aki & Chouet 1975). The decay of the coda waves with lapse time, or coda attenuation, is related to the distribution of scatterers (Sens-Schönfelder *et al.* 2009; Carcolé & Sato 2010). Techniques to simulate scattered waves and envelopes of the coda waves have been developed using, for example, a single scattering approximation (Sato 1977), radiative transfer theory (Hoshiba 1994; Wegler *et al.* 2006), and finite-difference methods (Frankel & Clayton 1986). The spatial sensitivity of seismic waves depends on wavelength, and hence we should employ an effective medium theory to model properly waveforms related to small-scale heterogeneities (Jordan 2015).

Small-scale heterogeneity is important for strong ground motion prediction. The deterministic limit in high-frequency ground

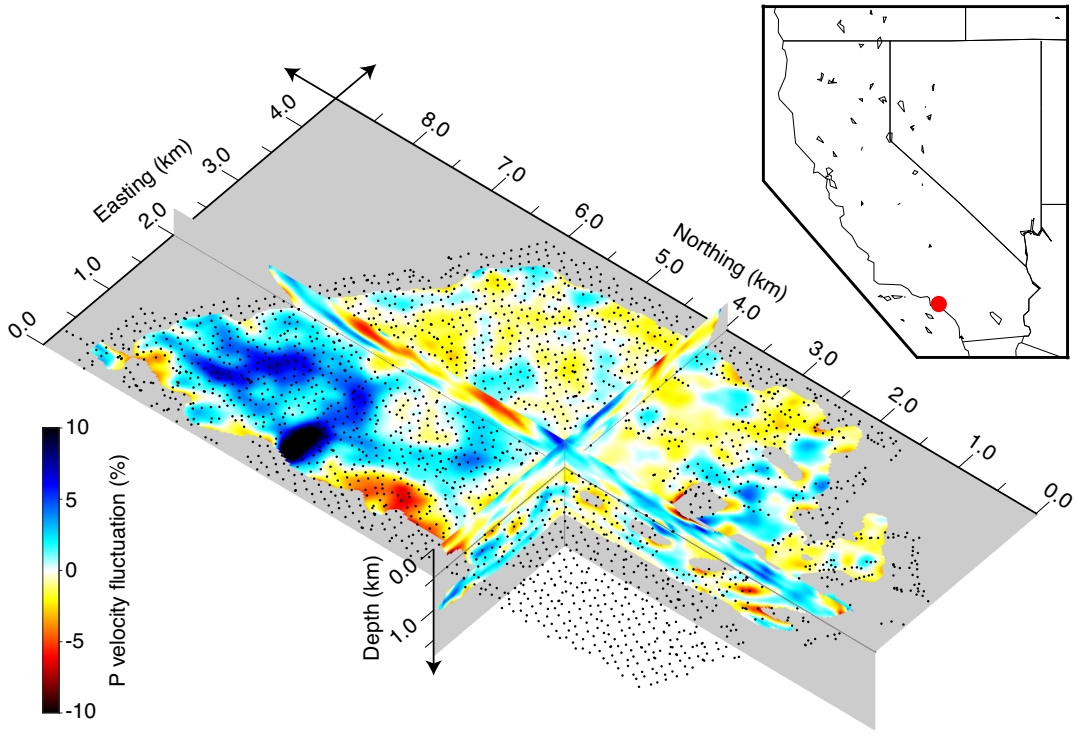

Figure 1. *P*-wave velocity model in 3-D view obtained from ambient seismic wavefields (Nakata *et al.* 2015). The colour illustrates the fractional fluctuation of *P*-wave velocities given by eq. (3), and cool colours indicate faster and warm colours indicate slower velocities than the laterally averaged velocity ($\bar{v}(z)$). The grey area shows poorly resolved areas according to the ray coverage of traveltime tomography. The black dots are the location of the stations projected at the depth of the horizontal slice (the stations are deployed at the ground surface). The red dot in the inset shows the location of the survey. The details of the velocity model are explained by Nakata *et al.* (2015).

motion simulations stands at about 1 Hz (Olsen *et al.* 1995). Above that, ground motions are typically simulated by assuming stochastic behaviour of time series (Beresnev & Atkinson 1997). Small-scale heterogeneities can be used for earthquake slip models to explain observed strong motion radiation (Mai & Beroza 2002). Recent studies have attempted to use statistical representations of fault roughness (Bydlon & Dunham 2015) and medium heterogeneity (Mai *et al.* 2010; Olsen & Takedatsu 2015) to push physics-based ground motion prediction to higher frequencies. To be successful, this effort requires reliable, quantitative information on the strength and variability of heterogeneity in the Earth's crust. We have that information at small scale length in some areas from well logs—vertically along the wellbore, and horizontally between wellbores (Olsen 2013; Shaw *et al.* 2014), but we lack it at spatial scales ranging from tens of metres to 10 km (i.e. mesoscale).

In this study, we consider the *P*-wave velocity structure (Fig. 1) estimated under Long Beach, California from the ambient seismic wavefield (Nakata *et al.* 2015). The Long Beach experiment contained about 2500 vertical-component geophones that continuously recorded ground motion. The dense array provides unique mesoscale information. Nakata *et al.* (2015) estimated the velocity model using *P*-wave traveltime tomography with a cell size of 25 × 25 × 25 m^3. Their results form the foundation for our study. First, we introduce a representation of random velocity structure using the autocorrelation function (ACF). Next, we estimate parameters of the ACF using the observed velocity structure. Finally, we validate synthetic coda envelopes based on the estimated ACF against the observed coda waves of a local earthquake.

STOCHASTIC RANDOM VELOCITY MODEL

If we assume that the randomness of a medium is spatially homogeneous, perhaps varying differently in different directions, we can characterize the stochastic nature of that medium using an ACF ($R(\boldsymbol{x})$, where $\boldsymbol{x}$ represents the spatial lag) (Ishimaru 1978). If we can define the ACF, then we can identify the character of randomness of a medium. The spatial lag $\boldsymbol{x}$ can represent any coordinate, but here we consider Cartesian coordinates for simplicity ($\boldsymbol{x} = (x, y, z)$). The power spectral density function (PSDF) of the random media is computed by the Fourier transform of the ACF over three spatial coordinates:

$$P(k_x, k_y, k_z) = \iiint_{-\infty}^{\infty} R(x, y, z) \mathrm{e}^{-k_x x - k_y y - k_z z}\, \mathrm{d}x\, \mathrm{d}y\, \mathrm{d}z, \tag{1}$$

where k is the wavenumber ($k = 2\pi/\lambda$, where λ is the wavelength) in each direction. For geophysical applications and particularly wave propagation problems, von Kármán, Gaussian, self-affine (fractal), and Kummer ACFs have been developed and used (Ishimaru 1978; Klimeš 2002; Sato *et al.* 2012). Based on data fitting as discussed below, we find that among these distributions, the von Kármán correlation function (P_{vK}) best represents our velocity data:

$$P_{\mathrm{vK}}(k_x, k_y, k_z) = \frac{2^d \pi^{d/2} \varepsilon^2 a_x a_y a_z \Gamma(\kappa + d/2)}{\Gamma(|\kappa|)\left(1 + a_x^2 k_x^2 + a_y^2 k_y^2 + a_z^2 k_z^2\right)^{\kappa + d/2}}, \tag{2}$$

where d is the Euclidean dimension ($d = 3$), Γ the gamma function, κ the Hurst exponent, a the correlation length for each direction, and ε the fractional magnitude of the fluctuation, which is given by $\varepsilon \equiv R(0, 0, 0)$. The PSDF of the von Kármán model follows a

power law (fractal randomness) for large wavenumbers ($ak \gg 1$), where κ controls the rate of the power-law decay with increasing wavenumber (Supporting Information Fig. S1). In contrast to the self-affine model, the von Kármán model has a low-cut wavenumber filter, and hence large-scale heterogeneities are not fractal.

We estimate the PSDF from the data of the 3-D velocity cube (Fig. 1). The velocity structure of the study area has a strong 1-D trend in depth. To make the mean of the random medium zero, we normalize the velocity model:

$$\xi(x, y, z) = \frac{v(x, y, z) - \bar{v}(z)}{\bar{v}(z)}, \tag{3}$$

where $\bar{v}(z)$ represents the 1-D trend, and the dimensionless function $\xi(x, y, z)$ is the perturbation of the velocities for which $\sum_{x,y,z}\xi(x, y, z) = 0$. The directions x and y are arbitrary horizontal directions, and here we choose easting and northing, respectively. We are free to choose the function $\bar{v}(z)$ as a constant, linear trend, or more complicated functions, provided we do not remove the heterogeneity of the model. We use a linear regression of the laterally averaged velocity model based on a least-squares fit similar to Shiomi *et al.* (1997), and show $\xi(x, y, z)$ in Fig. 1. Nakata *et al.* (2015) employed a boxcar smoothing filter to stabilize the inverted velocities in the tomography results we use. Because this filter provides an additional apparent decay in the PSDF, we compensate for this effect by deconvolving the PSDF of the filter (Shiomi *et al.* 1997). After deconvolution, the PSDF of the fractional velocity model (P_d) exhibits a greater vertical than horizontal extent of the high PSD (Fig. 2a), which suggests anisotropy of the heterogeneity as we discuss quantitatively below.

To reveal the statistical properties of the velocity structure, we compare the PSDF of the velocity model with von Kármán models, in which we estimate a_x, a_y, a_z, κ, and ε in eq. (2) to represent the data. Because the two horizontal directions are chosen arbitrarily, we assume $a_x = a_y = a_r$, and hence we have four independent parameters to estimate. In the supplemental material, we show the fit of other ACFs to the data as well. For our parameter estimation, we minimize a misfit based on the L_2 norm as

$$\text{Misfit} = \frac{1}{N}\left\{\sum_{\mathbf{k}}\left[w(\mathbf{k})\left\{\log_{10}(P_{\mathrm{vK}}(\mathbf{k})) - \log_{10}(P_\mathrm{d}(\mathbf{k}))\right\}^2\right]\right\}^{1/2}, \tag{4}$$

where w is a weighting function and N the total number of samples. Although the wavenumber is evenly sampled on a linear scale, the inversion is more stable when the wavenumber is evenly sampled on a logarithmic scale. The weighting function transforms the wavenumber sampling from a linear scale to logarithmic scale, which puts a greater weight on smaller wavenumbers. We constrain $\sum_{\mathbf{k}} w(\mathbf{k}) = 1.0$ to preserve the total intensity. For this parameter estimation, we do not use wavelengths shorter than 100 m, which approximates the average receiver spacing.

The data are better represented by the von Kármán model (Figs 2 and 3) compared with other ACF models (Supporting Information Fig. S2). This means that the velocity structure follows a power law at large wavenumbers. The parameters for the best von Kármán model are $(a_r, a_z, \kappa, \varepsilon) = (0.51\,\text{km}, 0.10\,\text{km}, 0.040, 0.107)$. Although we use a grid search to estimate the parameters (Fig. 4), based on the shape of the misfit function, we could have used a gradient method to reduce the computational cost. For our inversion, we have enough sensitivity to estimate a correlation length as short as 0.1 km. The correlation length defines the length at which fractal heterogeneity breaks down (transition zone is at $ak = 2\pi a/\lambda$), and we have sufficient wavenumber resolution ($ak = 0.1k < 1.0$; Fig. 3) to resolve the correlation length.

The aspect ratio of the correlation length is 5.1, which means that the heterogeneity in our study area is highly anisotropic at short wavelengths, with much shorter scale length vertically than horizontally. This anisotropy is to be expected for a layered sedimentary environment. The Hurst exponent of 0.04 indicates that the area is very rough and rich in short wavelength heterogeneities (fractal dimension of 3.96 (i.e. $d + 1 - 0.04$)). The vertical correlation length of 0.10 km, the Hurst exponent of 0.04, and the fractal magnitude of 0.107 are consistent with independent estimates from sonic logs (Olsen 2013).

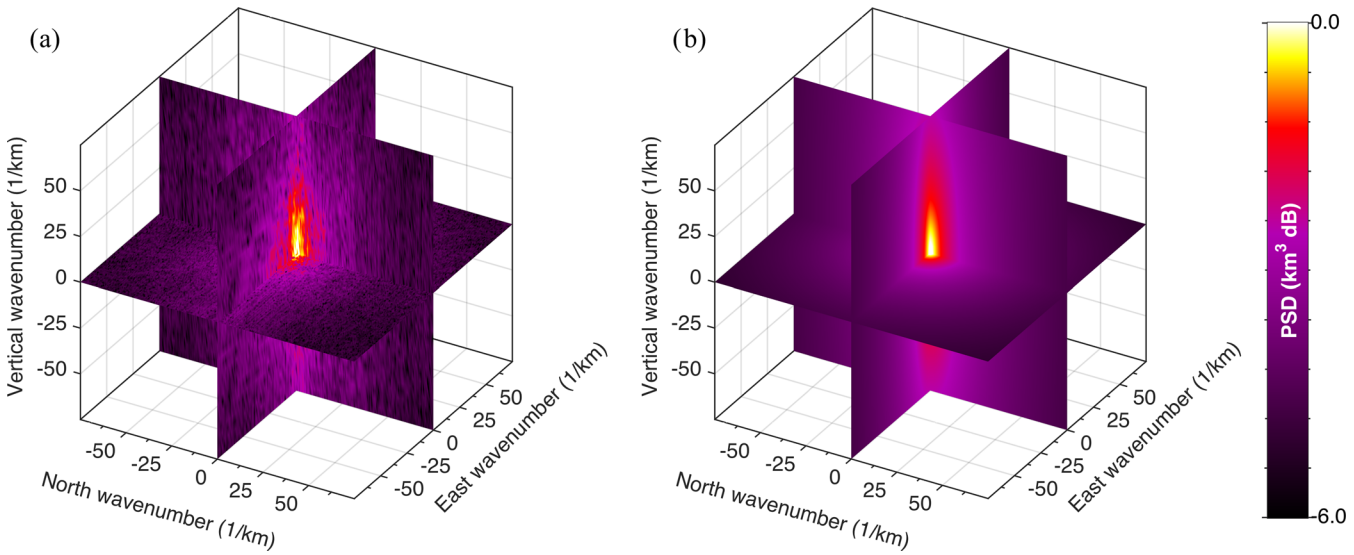

Figure 2. (a) Power spectra of the velocity model shown in Fig. 1 in the wavenumber domain. (b) Power spectra of the best-fit von Kármán model (a_r = 0.51 km, a_z = 0.10 km, κ = 0.040 and ε = 0.107).

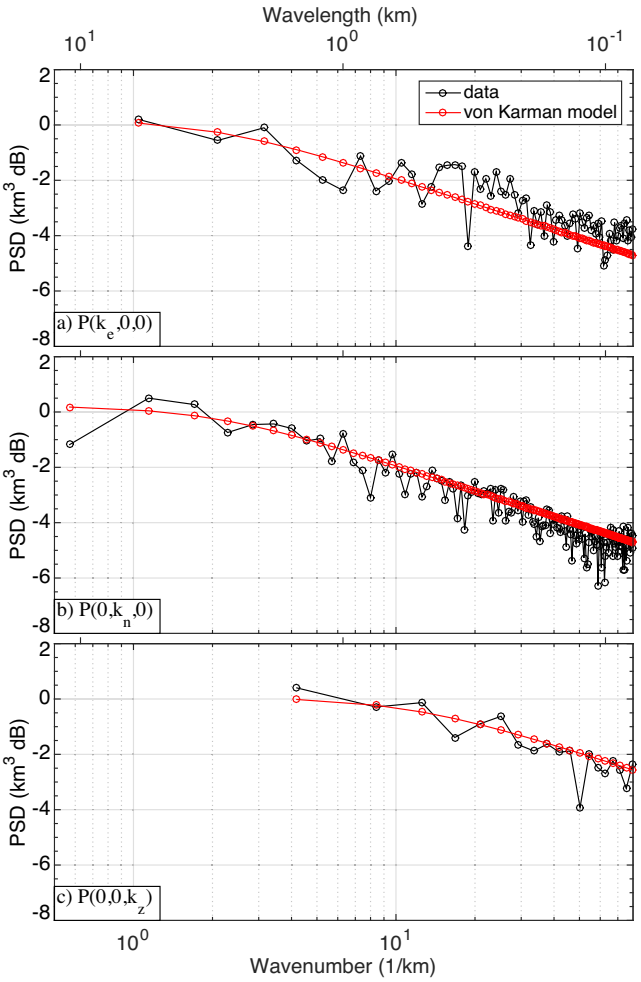

Figure 3. Comparison between the observed velocity model (black) and the best von Kármán model (red) along the (a) east-wavenumber (k_e), (b) north-wavenumber (k_n) and (c) vertical-wavenumber (k_z) axes in Fig. 2. Note: we show only the positive wavenumbers.

FITTING AN EARTHQUAKE CODA ENVELOPE

Coda waves have an important role in understanding the heterogeneity of the Earth (Aki 1969). Here, we perform a preliminary test through modelling of the envelope of an earthquake using the PSDF we obtained (Fig. 5). We use the closest earthquake to the array as an example; the earthquake is M_w 2.0 and occurred on 2012 March 7, 4.5 km to the east of the centre of the array at 11.1 km depth. We use receivers located 11.95–12.05 km away from the hypocentre of the earthquake and average envelopes of the observed wavefields over all receivers used. This averaging is important because we estimate the average stochastic model for the entire area in the previous section.

Several methods are available to model the coda envelope of the earthquake. For example, we could use a Markov approximation or radiative transfer theory, or we could numerically simulate the wavefield (Saito *et al.* 2003). Since we do not have information below the depth of the velocity model in Fig. 1 (i.e. below 1.2 km depth) and the estimated Hurst exponent is small, we employ radiative transfer theory to approximate the decay of the envelope. Because synthesizing the envelope of an anisotropic von Kármán model is still a research topic [for anisotropic Gaussian ACF, see Sato (2008)], we assume a 3-D isotropic ACF with a correlation length of $\sqrt{a_x^2 + a_y^2 + a_z^2}$. Other parameters ($\varepsilon$ and κ) are the same as used in Fig. 2(b). The large aspect ratio of the correlation length may increase wave scattering, which is partly guided by the stratified structure (Olsen 2013; Savran *et al.* 2014).

The scattering coefficient $g(\theta)$ of the estimated von Kármán PSDF with the isotropic scattering assumption is given by eq. (4.25) of Sato *et al.* (2012):

$$g(\theta) = \frac{1}{\pi}\left(\frac{\omega}{c}\right)^4 P\left(\frac{2\omega}{c}\sin\frac{\theta}{2}\right), \tag{5}$$

where ω is the angular frequency, θ the scattering angle, and c the mean wave velocity. We estimate the velocity in eq. (5) from the arrival times of the direct waves and use the central frequency of the each range as ω. The total scattering coefficient g_0, which is the inverse of the mean free path l, is obtained by the integral over the scattering angle:

$$g_0 = \frac{1}{2}\int_0^\pi \sin\theta\, g(\theta)\mathrm{d}\theta = \frac{1}{l}. \tag{6}$$

An approximate solution of the 3-D radiative transfer equation based on the given l is

$$P(r,t) \approx \frac{\mathrm{e}^{-ct/l}}{4\pi r^2}\delta(r-ct) + \frac{(1-r^2/c^2t^2)^{1/8}}{(4\pi lct/3)^{3/2}}\mathrm{e}^{-ct/l}G \times\left(\frac{ct}{l}\left[1-\frac{r^2}{c^2t^2}\right]^{3/4}\right)H(ct-r), \tag{7}$$

where

$$G(x) \approx \mathrm{e}^x\sqrt{1+2.026/x},$$

r is the distance from the source to the receiver, H is the Heaviside step function (0 for $ct - r < 0$ and 1 for $ct - r > 0$) to satisfy causality and δ the Dirac delta function (Paasschens 1997).

Using eqs (5)–(7) with the estimated PSDF P and velocity c, we can roughly simulate the envelopes of the earthquake coda. Because we consider one wave mode without converted waves in eq. (7) (i.e. scalar waves), we independently compute envelopes for P and S waves at 4–8 Hz and 8–16 Hz. One can compute the envelope with mode conversion based on the Born approximation (Maeda *et al.* 2008). To synthesize the envelopes for P and S waves, we give two parameters that are the amplitude of each wave and the length of the path of the heterogeneous layer (r). We estimate a common path length for all four envelopes but independent amplitude normalization. This assumption is equivalent to considering heterogeneous structure on top of a homogeneous half space, with coda waves only excited in the heterogeneous structure. To align the first break time of the envelopes with arrival times of the earthquake, we add traveltimes for the homogeneous region $(12.0 - r)/c$ to $P(r, t)$ in eq. (7).

The decay of the synthetic envelopes fit reasonably well to the observed ones, especially for S waves (Fig. 5). Note that the decays are governed by the heterogeneity of the model, which we estimated from the deterministic velocity model (Fig. 1). With the caveat that we did not use the anisotropic aspect of the velocity heterogeneity in this test, it is interesting to note that the energy of the body waves we extracted from ambient wavefields extended to 10 Hz (Nakata *et al.* 2015). Yet smaller-scale structure, which is extrapolated to higher wavenumbers, rather than inferred from the deterministic tomography, is consistent with the same heterogeneity spectrum in that it successfully predicts the coda decay (Fig. 5). Because we do not include any reflectors or deterministic structure for simulating

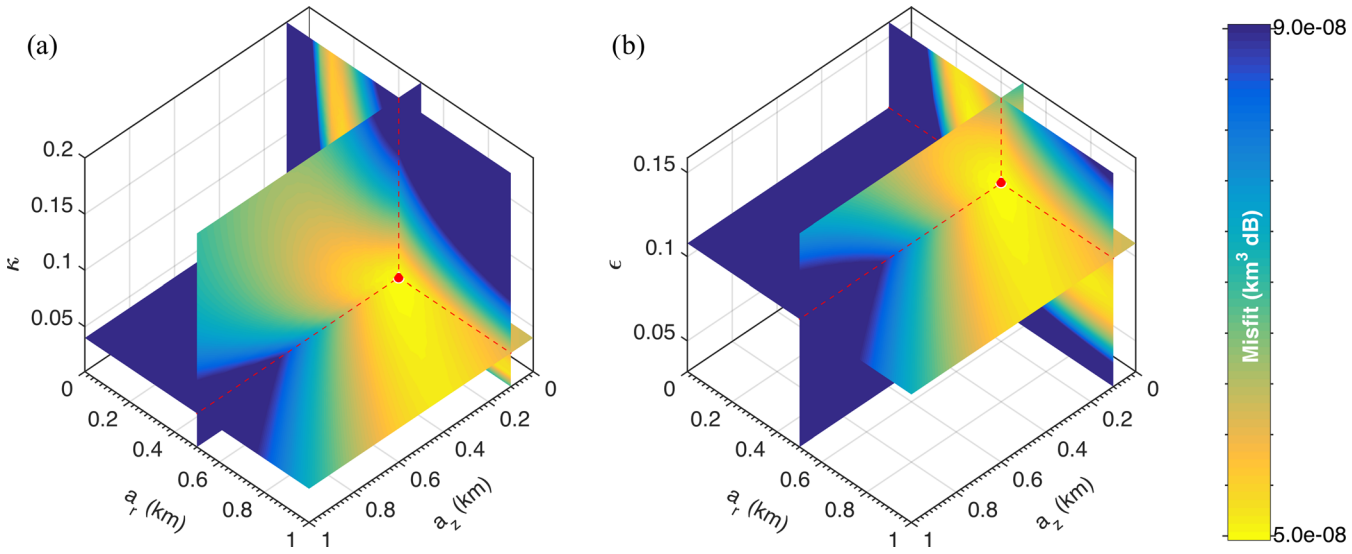

Figure 4. 4-D misfit function of the von Kármán model (eq. 4). Each panel shows the misfit cube of three parameters. We choose the best-fitted parameter of the remaining parameter for each panel (e.g. $\varepsilon = 0.107$ for panel (a)). The red dot shows the parameters for the model in Fig. 2(b).

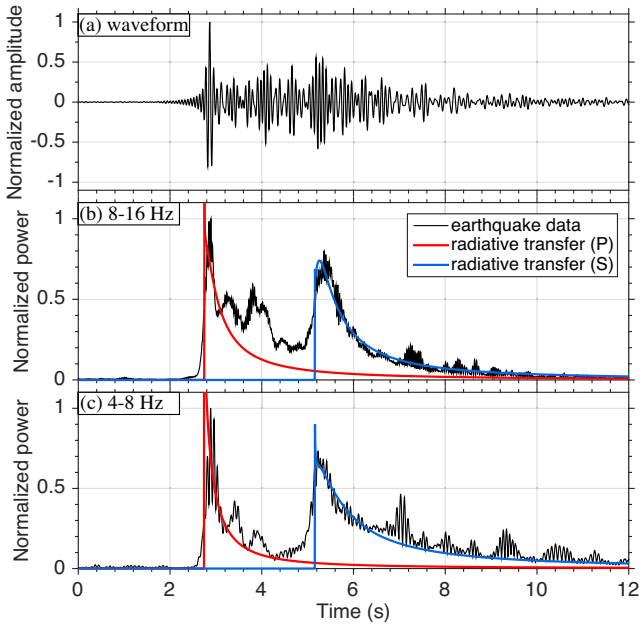

Figure 5. (a) An example of waveforms generated by the nearby earthquake (4.5 km east and 11.1 km deep) at one station (0.5–16 Hz) and (b,c) mean-square envelope of the earthquake waveforms compared with the synthetic envelopes computed by radiative transfer theory with the estimated von Kármán model at the frequency ranges of (b) 8–16 Hz and (c) 4–8 Hz (using an isotropic random model with correlation length of $\sqrt{a_x^2 + a_y^2 + a_z^2}$). Radiative transfer theory is based on scalar waves and the envelopes for *P* and *S* waves (red and blue lines, respectively) are computed separately. The thicknesses of the assumed heterogeneous medium for the envelopes are 1.5 km for both frequency ranges. The earthquake envelope is averaged over receivers that are located at 11.95–12.05 km from the hypocentre based on straight ray paths.

envelopes, we cannot model non-direct ballistic waves at shorter wavelengths. Also, radiative transfer theory is not sensitive to forward scattered waves, which may be small in this medium because κ is small. To improve the modelling, we could use, for example, a hybrid method of radiative transfer theory and a Markov approximation (Saito *et al.* 2003).

DISCUSSION AND CONCLUSIONS

We estimate the statistical characteristics of the *P*-wave velocity heterogeneity at Long Beach, California. The heterogeneity is fit well with a von Kármán random model with ellipsoidal anisotropy. The short-wavelength structure follows power-law scaling (fractal dimension of 3.96), and therefore the von Kármán model is suitable for the stochastic representation of the velocity structure. We find that the heterogeneity of the area is highly anisotropic, and the aspect ratio (horizontal/vertical) of the anisotropy is 5.1. The method used here could be applied to other areas where dense arrays have been deployed.

The decay of the coda envelopes computed by the estimated PSDF of the random model approximates the coda waves of a nearby earthquake. This result supports our estimated PSDF for the study area. We use the velocity model that is estimated by deterministic ray-based tomography. As discussed by Nolet & Dahlen (2000), tomography is less sensitive for structure that is smaller than the wavelength; however, if we can explain the envelopes of coda waves at higher frequencies/shorter wavelengths, we can overcome this limitation of resolution. To confirm this hypothesis, we need to understand to what extent the heterogeneity of the Earth really follows the von Kármán model in which the structure smaller than $2\pi\lambda$ satisfies a power law, which is an important question for future research.

ACKNOWLEDGEMENTS

We are grateful for Haruo Sato at Tohoku University for fruitful discussion to understand the ACFs. We thank Signal Hill Petroleum, Inc. and NodalSeismic for providing ambient noise data at Long Beach, and Jason P. Chang at Stanford University for his work on the initial data processing. We thank the Center for Computational Earth and Environmental Science at Stanford University, the Stanford Research Computing Center and SuperMicro Inc. for computational resources. This study was supported by the Southern California Earthquake Center (SCEC). The SCEC is funded by NSF Cooperative Agreement EAR-1033462 and USGS Cooperative Agreement G12AC20038. The SCEC contribution number for this paper is 6012.

REFERENCES

Aki, K., 1969. Analysis of the seismic coda of local earthquakes as scattered waves, *J. geophys. Res.,* **74**(2), 615–631.

Aki, K. & Chouet, B., 1975. Origin of coda waves: Source, attenuation, and scattering effects, *J. geophys. Res.,* **80**(23), 3322–3342.

Aki, K., Christoffersson, A. & Husebye, E.S., 1976. Three-dimensional seismic structure of the lithosphere under Montana LASA, *Bull. seism. Soc. Am.,* **66**(2), 501–524.

Becker, T.W., Browaeys, J.T. & Jordan, T.H., 2007. Stochastic analysis of shear-wave splitting length scales, *Earth planet. Sci. Lett.,* **259,** 526–540.

Beresnev, I.A. & Atkinson, G.M., 1997. Modeling finite-fault radiation from the ω^n spectrum, *Bull. seism. Soc. Am.,* **87**(1), 67–84.

Bydlon, S.A. & Dunham, E.M., 2015. Rupture dynamics and ground motions from earthquakes in 2-D heterogeneous media, *Geophys. Res. Lett.,* **42**(6), 1701–1709.

Carcolé, E. & Sato, H., 2010. Spatial distribution of scattering loss and intrinsic absorption of short-period S waves in the lithospehre of Japan on the basis of the multiple lapse time window analysis of Hi-net data, *Geophys. J. Int.,* **180,** 268–290.

Frankel, A. & Clayton, R.W., 1986. Finite difference simulations of seismic scattering: Implications for the propagation of short-period seismic waves in the crust and models of crustal heterogeneity, *J. geophys. Res.,* **91**(B6), 6465–6489.

Goff, J.A. & Jordan, T.H., 1988. Stochastic modeling of seafloor morphology: Inversion of sea beam data for second-order statistics, *J. geophys. Res.,* **93**(B11), 13 589–13 608.

Gudmundsson, O., Davies, J.H. & Clayton, R.W., 1990. Stochastic analysis of global traveltime data: mantle heterogeneity and random errors in the ISC data, *Geophys. J. Int.,* **102,** 25–43.

Holliger, K., 1996. Upper-crustal seismic velocity heterogeneity as derived from a variety of P-wave sonic logs, *Geophys. J. Int.,* **125,** 813–829.

Holliger, K. & Levander, A.R., 1992. A stochastic view of lower crustal fabric based on evidence from the Ivrea Zone, *Geophys. Res. Lett.,* **19**(11), 1153–1156.

Holliger, K. & Levander, A., 1994. Lower crustal reflectivity modeled by rheological controls on mafic intrusions, *Geology,* **22,** 367–370.

Hoshiba, M., 1994. Simulation of coda wave envelope in depth dependent scattering and absorption structure, *Geophys. Res. Lett.,* **21**(25), 2853–2856.

Ishimaru, A., 1978. *Wave Propagation and Scattering in Random Media,* Academic Press, Inc.

Jordan, T.H., 2015. An effective medium theory for three-dimensional elastic heterogeneities, *Geophys. J. Int.,* **203,** 1343–1354.

Klimeš, L., 2002. Correlation functions of random media, *Pure appl. geophys.,* **159,** 1811–1831.

Levander, A.R. & Holliger, K., 1992. Small-scale heterogeneity and large-scale velocity structure of the continental crust, *J. geophys. Res.,* **97**(B6), 8797–8804.

Maeda, T., Sato, H. & Nishimura, T., 2008. Synthesis of coda wave envelopes in randomly inhomogeneous elastic media in a half-space: single scattering model including Rayleigh waves, *Geophys. J. Int.,* **172,** 130–154.

Mai, P.M. & Beroza, G.C., 2002. A spatial random field model to characterize complexity in earthquake slip, *J. geophys. Res.,* **107**(B11), ESE 10-1-ESE 10–21.

Mai, P.M., Imperatori, W. & Olsen, K.B., 2010. Hybrid broadband ground-motion simulations: Combining long-period deterministic synthetics with high-frequency multiple S-to-S backscattering, *Bull. seism. Soc. Am.,* **100**(5A), 2124–2142.

Nakata, N., Chang, J.P., Lawrence, J.F. & Boué, P., 2015. Body-wave extraction and tomography at Long Beach, California, with ambient-noise tomography, *J. geophys. Res.,* **120,** 1159–1173.

Nolet, G. & Dahlen, F.A., 2000. Wave front healing and the evolution of seismic delay times, *J. geophys. Res.,* **105**(B8), 19 043–19 054.

Olsen, K. & Takedatsu, R., 2015. The SDSU broadband ground-motion generation module BBtoolbox version 1.5, *Seismol. Res. Lett.,* **86**(1), 81–88.

Olsen, K.B., 2013. Statistical modeling of shallow velocity heterogeneities with validation against strong ground motion, Tech. Rep., US Geological Survey Final Technical Report for Award G12AP20015.

Olsen, K.B., Pechmann, J.C. & Schuster, G.T., 1995. Simulation of 3D elastic wave propagation in the Salt Lake Basin, *Bull. seism. Soc. Am.,* **85**(6), 1688–1710.

Paasschens, J.C.J., 1997. Solution of the time-dependent Boltzmann equation, *Phys. Rev. E,* **56**(1), 1135–1141.

Puster, P. & Jordan, T.H., 1997. How stratified is mantle convection?, *J. geophys. Res.,* **102**(B4), 7625–7646.

Saito, T., Sato, H., Fehler, M. & Ohtake, M., 2003. Simulating the envelope of scalar waves in 2D random media having power-law spectra of velocity fluctuation, *Bull. seism. Soc. Am.,* **93**(1), 240–252.

Sato, H., 1977. Energy propagation including scattering effects single isotropic scattering approximation, *J. Phys. Earth,* **25,** 27–41.

Sato, H., 2008. Synthesis of vector-wave envelopes in 3-D random media characterized by a nonisotropic Gaussian ACF based on the Markov approximation, *J. geophys. Res.,* **113,** B08,304, doi:10.1029/2007JB005524.

Sato, H., Fehler, M.C. & Maeda, T., 2012. *Seismic Wave Propagation and Scattering in the Heterogeneous Earth,* 2 edn, Springer.

Savran, W., Olsen, K.B. & Jacobsen, B.H., 2014. Unique amplification patterns generated by models of small-scale crustal heterogeneities, in *AGU Fall Meeting,* S41E-06, San Francisco, CA.

Sens-Schönfelder, C., Margerin, L. & Campillo, M., 2009. Laterally heterogeneous scattering explains Lg blockage in the Pyrenees, *J. geophys. Res.,* **114,** B07,309, doi:10.1029/2008JB006107.

Shaw, J.H., Jordan, T.H. & Pleasch, A., 2014. Toward implementation of a stochastic description of fine scale basin velocity structure in the SCEC Community Velocity Model (CVM-H), Tech. Rep., SCEC report 14176.

Shiomi, K., Sato, H. & Ohtake, M., 1997. Broad-band power-law spectra of well-log data in Japan, *Geophys. J. Int.,* **130,** 57–64.

Wegler, U., Korn, M. & Przybilla, J., 2006. Modeling full seismogram envelopes using radiative transfer theory with Born scattering coefficients, *Pure appl. geophys.,* **163,** 503–531.

SUPPORTING INFORMATION

Additional Supporting Information may be found in the online version of this paper:

Figure S1. PSDFs of four models (Klimeš, 2002; Sato *et al.*, 2012). The correlation length (for both Gaussian and von Kármán), Hurst exponents and the intensity of the randomness are identical for all models. The vertical black dotted line indicates the inverse of the autocorrelation length used to compute the PSDFs (1/0.51 km^{-1}).
Figure S2. Best-fit PSDFs for the velocity data shown in Fig. 2(a) using (a) Gaussian, (b) Kummer and (c) self-affine correlation functions (http://gji.oxfordjournals.org/lookup/suppl/doi:10.1093/gji/ggv421/-/DC1).

Please note: Oxford University Press is not responsible for the content or functionality of any supporting materials supplied by the authors. Any queries (other than missing material) should be directed to the corresponding author for the paper.